

1
2
3
4
5
6
7
8
9
10
11
12
13
14
15
16
17
18
19
20
21
22
23
24
25
26
27
28

Supplementary Information

Liquid phase IR detector based on photothermal effect of reduced graphene oxide doped liquid crystal

Mohammad A. Adeshina^a, Hakseon Lee^a, BharathKumar Mareddi^b, Daekyung Kang^c, Abdulazeez M. Ogunleye^a, Hyunmin Kim^d, Taewan Kim^e, Muhan Choi^a, Hongsik Park^a, and Jonghoo Park^{a†}

^a School of Electronic and Electrical Engineering, Kyungpook National University, Daegu 41566, Republic of Korea

^bIMEC, Leuven, Department of Electrical Engineering, KU Leuven, Leuven 3001, Belgium

^cDepartment of Biomedical Convergence Science and Technology, Kyungpook National University, Daegu41566, Republic of Korea.

^dCompanion Diagnostics & Medical Technology Research group DGIST, Daegu42988, Republic of Korea

^eDepartment of Electrical Engineering and Smart Grid Research Center Jeonbuk National University, Jeonju 54896, Korea

† Corresponding author Professor Jonghoo Park E-mail: jonghoopark@knu.ac.kr.

29

30 Synthesis of reduced graphene oxide

31 The reduced graphene oxide (rGO) was synthesized by reducing GO produced from the graphite powder
32 using the modified hummers method. 2 g of graphite with a mean size of 200 mesh and purity of 99%, 2 g
33 of sodium nitrate (NaNO_3), and 100 ml of sulfuric acid (H_2SO_4) with 95 weight percent (wt%) were mixed
34 and stirred for 1 hour. Upon cooling down the solution in an ice bath, 10 g of potassium permanganate
35 (KMnO_4) was added and magnetically stirred until the solution turned brown. While the stirring continued,
36 300 ml of deionized water was slowly added followed by 10 ml of hydrogen peroxide (H_2O_2) to eliminate
37 excess KMnO_4 . Deionized (DI) water was then added and centrifuged 5 times to remove the supernatant
38 and wash off the residuals. To make GO powder, the GO solution was dried in an oven at 80°C for 3 hours.
39 In the next step, 1 g of GO was dissolved in 400 ml of DI water using a sonicator bath. The GO solution
40 was heated to 100°C , then 10 ml of hydrazine was added and heated for 1 hour. The obtained rGO was
41 then washed using DI water and dried in the oven at 80°C for 3 hours. In the final step, 1 g of rGO was
42 dissolved in 100 ml of isopropyl alcohol and mixed using a rotating mixer for 10 minutes followed by the
43 solution ball milling for 2 hours.

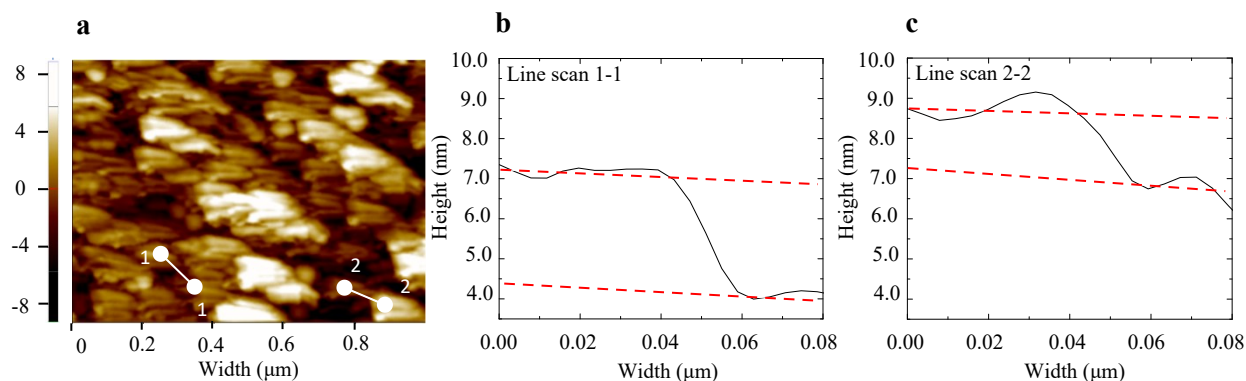


Figure S1 a) Atomic force microscopy image of reduced graphene oxide (rGO), with the corresponding rGO line scan chart b) (1-1) showing a thickness of 2.8nm (4 layers), and c) (2-2) with a thickness of 1.4nm (2 layers).

44 Atomic force microscopy measurement of rGO

45 The rGO thickness was measured using atomic force microscopy depicted in **Figure S1**. The measured
46 thickness of 2.8 and 1.52 nm observed with line scans 1-1 and 2-2 represent 4 and 2 layers of rGO
47 respectively. The thickness of a reduced graphene oxide is reported to be between 0.5 and 0.7 nm.¹⁻³

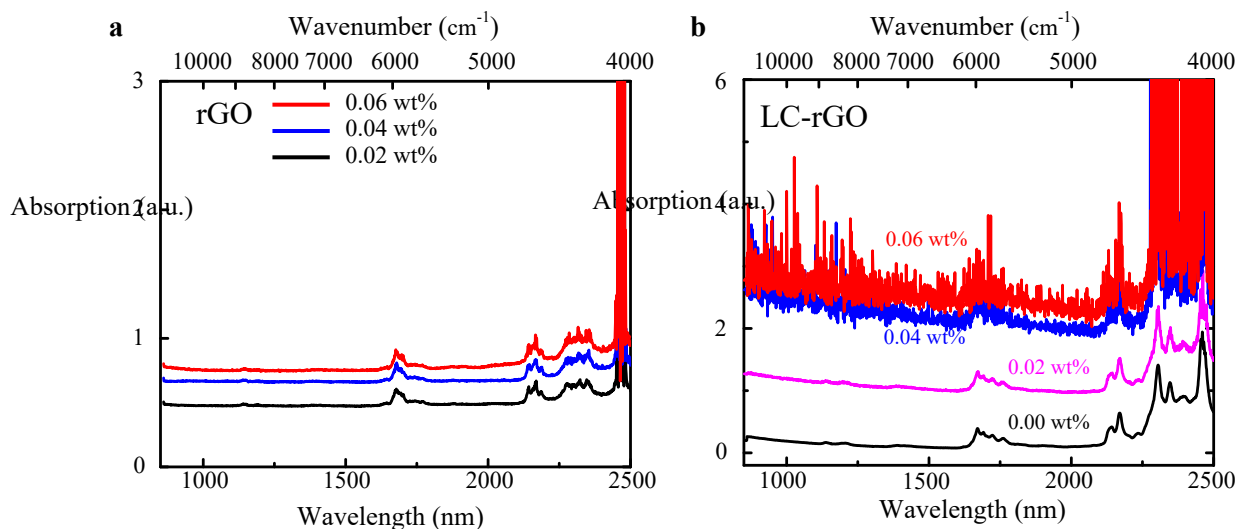


Figure S2. IR absorption spectra of a) reduced graphene oxide (rGO) with different weight concentration in toluene and b) 5CB nematic liquid crystal (LC)-rGO with different rGO doping concentration.

48 IR absorption of rGO, pure LC and LC-rGO

49 **Figure S2a** shows the IR absorption spectra of rGO with different weight percents dissolved in toluene.
50 Aside from having IR absorption peaks similar to pure LC, it demonstrates an increase in absorption peak
51 with increase in concentration. **Figure S2b** shows the IR absorption spectra of the pure liquid crystal (LC)
52 and LC-rGO with different rGO doping concentration. As the doping concentration increases, the IR
53 absorption in the entire wavelength range increases. LC-rGO with doping concentration of 0.06 wt%
54 exhibits significant IR absorption enhancement in the range of 2200-2500 nm.

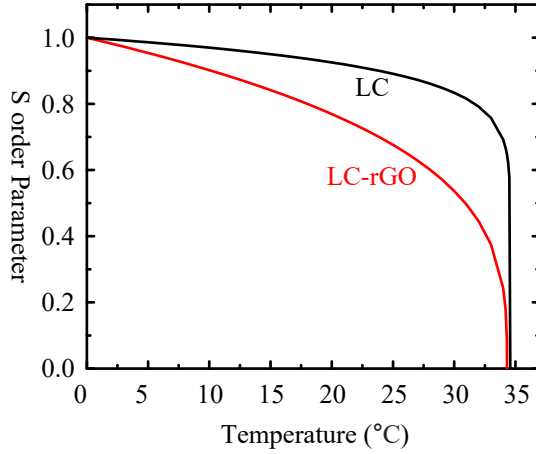


Figure S3. Order parameter of pure liquid crystal (LC) and LC-reduced graphene oxide (rGO) with beta (β) value of 0.09 and 0.3, respectively.

55 **Orientalional order parameter of the pure LC and LC-rGO**

56 **Figure S3** shows the order parameter as a function of temperature for pure LC and LC-rGO calculated
 57 based on the Haller's empirical expression⁴ stated in equation (1). The beta (β) value of 0.09 and 0.3 were
 58 assigned for the pure LC and LC-rGO, respectively, to resemble the differential scanning calorimetry (DSC)
 59 characteristics shown in **Figure S4**. The LC-rGO shows a higher rate of change in order parameter in the
 60 temperature range for nematic phase.⁵

$$S = \left(1 - \frac{T}{T_{NI}}\right)^\beta, \quad (1)$$

61 where the T and T_{NI} are LC temperature and nematic to isotropic transition temperature, respectively, and β
 62 is a unitless fitting parameter.

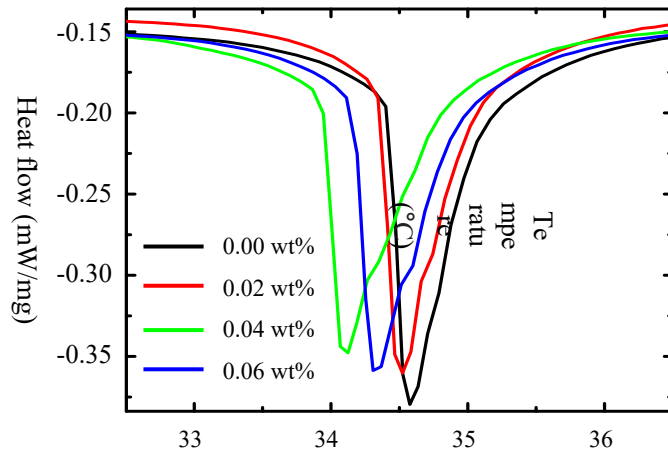


Figure S4. DSC data of pure liquid crystal (LC) and LC-reduced graphene oxide (rGO) with different rGO concentration.

63 DSC measurement of pure LC and LC-rGO

64 **Figure S4** shows the differential scanning calorimetry (DSC) results for the pure LC and LC-rGO with
 65 different doping concentrations. Doping rGO results in decreased phase transition temperature and different
 66 slope of heat flow with respect to the temperature. The phase transition temperature of the pure LC, 0.02
 67 wt% LC-rGO, 0.04 wt% LC-rGO, and 0.06 wt% LC-rGO were 34.58 °C, 34.52 °C, 34.12 °C, and 34.13
 68 °C, respectively.

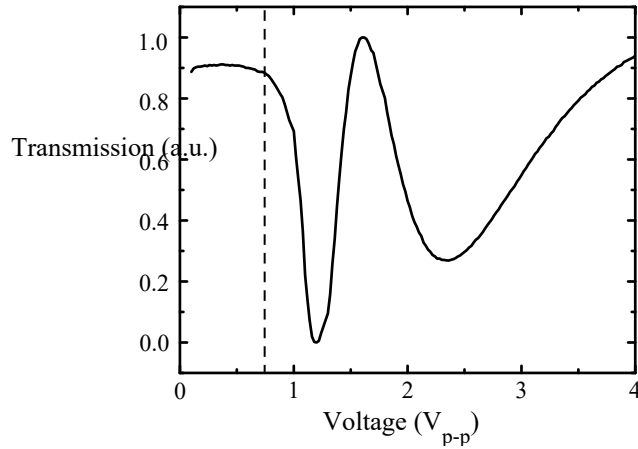


Figure S5. Voltage dependent transmission of 0.06 wt% liquid crystal (LC)-reduced graphene oxide (rGO) cell.

69 Voltage dependent optical transmission of LC-rGO

70 **Figure S5** shows the voltage dependent transmission of the 0.06 wt% LC-rGO cell. The optical
 71 transmission oscillates between minimum and maximum value as a function of the applied voltage higher
 72 than the threshold voltage of $750 \text{ mV}_{\text{p-p}}$. The surface anchoring energy is minimized close to this voltage.
 73 Because of this, LC molecules are easily reoriented as the temperature increases induced by the
 74 photothermal effect of the rGO. The measurement setup was described in a previous study.⁶

75 Correlation between the intensity and temperature

76 In **Figure 4b**, the following mathematical relationships in equation (2)-(4) were utilized to transform the
 77 intensity modulation to temperature modulation.

$$I = 151 - \alpha t, \quad (2)$$

$$T = 26.4 + \beta t, \quad (3)$$

$$\Delta T = \beta \left[\frac{\Delta I}{\alpha} \right], \quad (4)$$

78 where I and ΔI are intensity and change in intensity, respectively. T and ΔT are temperature and change in
79 temperature, respectively. t is time, α and β are slopes of intensity and temperature, respectively. The slope
80 of the intensity ($\alpha = -4.73$) and temperature ($\beta = 0.15$) as a function of time were obtained by linear fitting
81 of the data for the first 10s in Figure 2d.

82 References.

83 1 L. Rui, J. Liu, J. Li, Y. Weng, Y. Dou, B. Yuan, K. Yang and Y. Ma, *Biochim. Biophys. Acta (BBA)-*
84 *Biomembranes*, 2015, **1848**, 1203–1211.

85 2 P. Solís-Fernández, J. I. Paredes, S. Villar-Rodil, A. Martínez-Alonso and J. M. D. Tascón, *Carbon*
86 *N. Y.*, 2010, **48**, 2657–2660.

87 3 X. Jiao, Y. Qiu, L. Zhang and X. Zhang, *RSC Adv.*, 2017, **7**, 52337–52344.

88 4 I. Haller, *THERMODYNAMIC AND STATIC PROPERTIES OF LIQUID CRYSTALS*, Pergamon
89 Press, 1975, vol. 10.

90 5 T. M. Alam and C. J. Pearce, *Chem. Phys. Lett.*, 2014, **592**, 7–13.

91 6 M. B. Kumar, D. Kang, J. Jung, H. Park, J. Hahn, M. Choi, J. H. Bae, H. Kim and J. Park, *Opt. Lasers*
92 *Eng.*, 2020, **128**, 106006.

93